Solution Structure of the *N*-(Deoxyguanosin-8-yl)-1-aminopyrene ([AP]dG) Adduct Opposite dA in a DNA Duplex†

Zhengtian Gu,‡ Andrey Gorin,‡ Ramji Krishnasamy,§ Brian E. Hingerty,|| Ashis K. Basu,§ Suse Broyde,⊥ and Dinshaw J. Patel*,‡

Cellular Biochemistry and Biophysics Program, Memorial Sloan-Kettering Cancer Center, New York, New York 10021, Chemistry Department, University of Connecticut, Storrs, Connecticut 06269, Life Sciences Division, Oak Ridge National Laboratory, Oak Ridge, Tennessee 37831, and the Biology Department, New York University, New York, New York 10003

Received May 26, 1999

ABSTRACT: Solution structural studies have been undertaken on the aminopyrene-C^8-dG ([AP]dG) adduct in the d(C5−[AP]G6−C7)·d(G16−A17−G18) sequence context in an 11-mer duplex with dA opposite [AP]dG, using proton−proton distance and intensity restraints derived from NMR data in combination with distance-restrained molecular mechanics and intensity-restrained relaxation matrix refinement calculations. The exchangeable and nonexchangeable protons of the aminopyrene and the nucleic acid were assigned following analysis of two-dimensional NMR data sets on the [AP]dG·dA 11-mer duplex in H_2O and D_2O solution. The broadening of several resonances within the d(G16−A17−G18) segment positioned opposite the [AP]dG6 lesion site resulted in weaker NOEs, involving these protons in the adduct duplex. Both proton and carbon NMR data are consistent with a *syn* glycosidic torsion angle for the [AP]dG6 residue in the adduct duplex. The aminopyrene ring of [AP]dG6 is intercalated into the DNA helix between intact Watson−Crick dC5·dG18 and dC7·dG16 base pairs and is in contact with dC5, dC7, dG16, dA17, and dG18 residues that form a hydrophobic pocket around it. The intercalated AP ring of [AP]dG6 stacks over the purine ring of dG16 and, to a lesser extent dG18, while the looped out deoxyguanosine ring of [AP]dG6 stacks over dC5 in the solution structure of the adduct duplex. The dA17 base opposite the adduct site is not looped out of the helix but rather participates in an in-plane platform with adjacent dG18 in some of the refined structures of the adduct duplex. The solution structures are quite different for the [AP]dG·dA 11-mer duplex containing the larger aminopyrene ring (reported in this study) relative to the previously published [AF]dG·dA 11-mer duplex containing the smaller aminofluorene ring (Norman et al., *Biochemistry 28*, 7462−7476, 1989) in the same sequence context. Both the modified *syn* guanine and the dA positioned opposite it are stacked into the helix with the aminofluorene chromophore displaced into the minor groove in the latter adduct duplex. By contrast, the aminopyrenyl ring participates in an intercalated base-displaced structure in the present study of the [AP]-dG·dA 11-mer duplex and in a previously published study of the [AP]dG·dC 11-mer duplex (Mao et al., *Biochemistry 35*, 12659−12670, 1996). Such intercalated base-displaced structures without hydrogen bonding between the [AP]dG adduct and dC or mismatched dA residues positioned opposite it, if present at a replication fork, may cause polymerase stalling and formation of a slipped intermediate that could produce frameshift mutations, the most dominant mutagenic consequence of the [AP]dG lesion.

Nitropyrenes have been detected in a variety of environmental samples, including urban air particulate, coal fly ash, and automobile exhaust (*1*−*3*). 1-Nitropyrene (1-NP),[1] a representative of this class of compounds, is the most abundant nitroaromatic compound in the environment. It has also been detected in certain food items, such as grilled chicken and tea (*4*, *5*). Exposure to nitropyrenes is a concern because many compounds in this group are mutagenic in bacterial and mammalian cells (*1*, *6*, *7*) and tumorigenic in animals (*8*−*10*). Nitroreduction is a major pathway by which these compounds are metabolized (*11*, *12*). In both mammalian cells and bacteria, a major DNA adduct formed by 1-NP upon nitroreduction is *N*-(deoxyguanosin-8-yl)-1-aminopyrene ([AP]dG) (Figure 1a) (*11*, *12*). Both random and site-specific mutagenesis studies *in vivo* have suggested that this adduct is mutagenic (*13*−*16*). In a forward mutation assay, DNA sequence analysis of mutants induced by 1-NP via the reductive pathway in the lambda *c*I gene of *Escherichia coli uvr*-lysogen showed that ∼70% of mutants were

† This research is supported by NIH Grant CA-49982 to D.J.P., by NIH Grants CA-28038, CA-75449, and RR-06458 and DOE Grant DE-FG02-90ER60931 to S.B., by DOE Contract DE-AC05-960R22464 with Lockheed Martin Energy Research to B.E.H., and by NIH Grants ES07946 and ES09127 to A.K.B.

* Corresponding author. Telephone: 212-639-7207. FAX: 212-717-3066. E-mail: pateld@mskcc.org.

‡ Memorial Sloan-Kettering Cancer Center.

§ University of Connecticut.

|| Oak Ridge National Laboratory.

⊥ New York University.

[1] Abbreviations: AP, aminopyrene; [AP]dG, *N*-(deoxyguanosin-8-yl)-1-aminopyrene; COSY, correlation spectroscopy; NMR, nuclear magnetic resonance; NOESY, nuclear Overhauser enhancement spectroscopy; 1-NP, 1-nitropyrene; TOCSY, total correlation spectroscopy.

10.1021/bi9912138 CCC: $18.00
Published on Web 07/27/1999

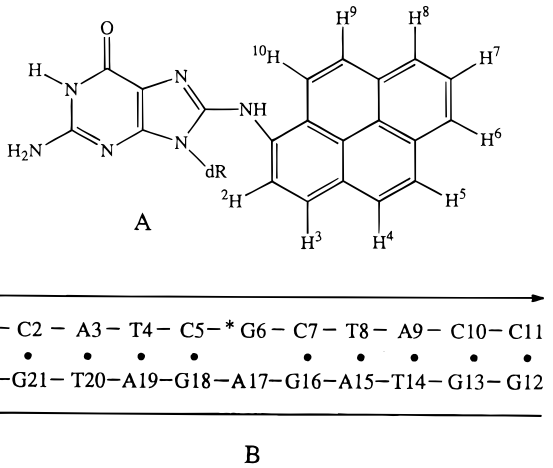

FIGURE 1: (A) The chemical formula of the *N*-(deoxyguanosiny-8-yl)-1-aminopyrene ([AP]dG) adduct. (B) The sequence of the [AP]dG·dA 11-mer duplex.

one-base deletions or additions (*13*). In a subsequent study in pBR322, −1 deletions and all the targeted base substitutions were observed, but +1 additions were not detected (*14*). Reductively activated 1-NP mutagenesis in *E. coli* was also studied in single stranded DNA (*15*). In the latter study, a major fraction of mutagenesis, and specifically one-base deletions and insertions, occurred in 5′-d(CG), 5′-d(GC), and 5′-d(GG) sequences. Each of the above three investigations established that base substitutions, and particularly dG to dT substitutions, also occurred at a significant frequency, albeit much lower than the frameshifts. In a site-specific study in the $d(CG)_3$ sequence, [AP]dG induced only frameshift mutations in *E. coli* (*16*). In contrast to the studies in bacteria, sequence analyses of mutants in mammalian cells indicated that base pair substitutions, specifically dG·dC to dT·dA transversions, occurred preferentially by reductively activated 1-NP (*17*, *18*). However, in human T-cells dG·dC to dT·dA transitions are the most common mutations (*6*). It is unclear at this time why the kinds of mutations detected in mammalian cells are so different from those in bacteria. Although multiple distinctions between the two systems may contribute, absence of an SOS type response in mammalian cells would probably provide the most reasonable explanation for the different mutagenic outcomes. Recent studies with the C^8 guanine adduct of 2-acetylaminofluorene strongly suggest that elongation of a slipped frameshift intermediate in bacteria requires an umuDC-independent, as yet biochemically uncharacterized, SOS function (*19*). Although there is no direct evidence either in favor or against the existence of such SOS functions in mammalian cells, it is conceivable that the lack of these regulatory proteins may be responsible for the low level of frameshift mutagenesis by AAF and AP adducts in mammalian systems. In addition, mammalian repair of premutagenic intermediates may be more efficient in removing frameshift than substitution intermediates. Further studies are needed to clarify these issues.

The structure of the [AP]dG adduct as manifested in the relative orientations of the AP and modified dG rings is likely to have a profound impact on its biological effects. Therefore, we have embarked upon a series of NMR-computational investigations of this adduct in a defined sequence context as a function of base positioned opposite the lesion site. The current inverstigation reports on the solution structure of the modified [AP]dG adduct (Figure 1A) positioned opposite dA in the [AP]dG·dA 11-mer duplex (Figure 1B). These structural studies establish that the modified dG ring of [AP]-dG in a *syn* alignment is displaced into the major groove, the aminopyrene ring is intercalated in its place between the intact flanking dG·dC base pairs, and the dA base located opposite the adduct on the partner strand participates in a novel in-plane platform with its 3′-linked neighbor in some refined structures of the [AP]dG·dA 11-mer duplex. These results are compared with the solution structure of the [AP]-dG adduct positioned opposite dC in the same sequence context in the corresponding [AP]dG·dC 11-mer duplex (*20*). The results are also compared with the solution structure of the *N*-(deoxyguanosin-8-yl)-1-aminofluorene ([AF]dG) adduct positioned opposite dA in the same sequence context in the [AF]dG·dA 11-mer duplex (*21*).

MATERIALS AND METHODS

Materials. The deoxyoligonucleotides d(C−C−A−T−C−G−C−T−A−C−C) and d(G−G−T−A−G−A−G−A−T−G−G) were synthesized on an Applied Biosystems Model 392 DNA synthesizer and purified by reverse-phase HPLC, as reported previously (*20*).

The preparation and purification of the [AP]dG containing 11-mer were carried out as reported previously (*22*, *23*). The d(C−C−A−T−C−[AP]G−C−T−A−C−C) 11-mer strand was annealed with the complementary d(G−G−T−A−G−A−G−A−T−G−G) 11-mer strand at 1 °C, and the stoichiometry was followed by monitoring single proton resonances in both strands by NMR spectroscopy.

NMR Experiments. All one- and two-dimensional NMR spectra were recorded on Varian Unity plus 600 and 500 MHz NMR spectrometers. A combination of through-space nuclear Overhauser effect (NOESY) and through-bond-correlated (COSY and TOCSY) two-dimensional spectra were recorded in the States-TPPI mode (*24*) on approximately 4 mg of [AP]dG·dA 11-mer duplex in 0.5 mL aqueous buffer (100 mM NaCl, 10 mM phosphate, pH 7.0 or pH 5.0) at 25 °C and 1 °C and analyzed to assign the aminopyrene and nucleic acid protons in the [AP]dG·dA 11 mer duplex. The NOESY spectrum (150 ms mixing time) of the adduct duplex in H_2O buffer at 1 °C was collected using a jump-return pulse for solvent suppression. NOESY spectra (50, 100, 150, and 200 ms mixing times) were collected to provide NOE buildup data on the adduct duplex in D_2O buffer at 25 °C with a relaxation delay of 2.5 s. The through-bond TOCSY data sets on the adduct duplex in D_2O buffer were recorded at spin lock times of 40 and 80 ms at 25 °C.

The indirect proton−phosphorus correlation spectrum was recorded on the [AP]dG·dA 11-mer duplex in D_2O at 25 °C using the pulse sequence described previously (*25*). The phosphorus spectra were referenced relative to external 10% trimethyl phosphate (TMP). The $^1H-^{13}C$ HMQC correlation spectra on the [AP]dG·dA 11-mer duplex in D_2O buffer were also recorded at 25 °C. The carbon spectra were referenced relative to external 3-(trimethylsilyl)propionate (TSP) using the calibration method described previously (*26*).

The base proton to sugar H1′ NOE cross-peaks in the shortest mixing time NOESY data set in D_2O were evaluated to qualitatively differentiate *syn* and *anti* glycosidic torsion

angles (*27*). The proton−proton vicinal coupling constants among sugar protons were analyzed from phase-sensitive COSY data to qualitatively distinguish between the C3′-*endo* and C2′-*endo* family of sugar puckers (*28*).

Structure Calculations. We have performed two stage calculations to obtain the solution structure of the [AP]dG·dA 11-mer duplex: (1) minimized potential energy calculations were carried out with DUPLEX, a molecular mechanics program for nucleic acids that performs potential energy minimizations in the reduced variable domain of torsion angle space (*29*), (2) the structures from stage 1 distance-restrained molecular mechanics computations were next subjected to intensity-restrained relaxation matrix refinement computations to take into account contributions from spin diffussion.

Distance-Restrained Molecular Mechanics Refinement. The molecular mechanics DUPLEX program uses a potential set similar to the one developed by Olson and co-workers for nucleic acids (*30*). Geometry and force field parameters, including partial charges, for the [AP]dG adduct were the same as those employed previously (*23*). The DUPLEX computational protocol is similar to that reported previously in our study of the [AP]dG·dC 11-mer duplex (*20*). These DUPLEX calculations were carried out at the NSF San Diego Supercomputer Center and the DOE National Energy Research Supercomputer Center.

The calculation of interproton distance bounds using volume build-up of NOE cross-peaks was based on the two spin approximation using the dT(NH3)−dA(H2) fixed distance of 2.92 Å for the NOESY data set in H_2O solution and the dC(H5)−dC(H6) fixed distance of 2.45 Å for the NOESY data sets in D_2O solution. The upper and lower bound ranges on the estimated interproton distances for nonexchangeable protons were determined based on the resolution of the cross-peaks in the two-dimensional contour plots and the quality of the NOE build-up plots. However, several cross-peaks between protons located at or close to the lesion site were somewhat broadened significantly and wider bounds were used.

Relaxation Matrix Refinement. Two final energy minimized structures obtained from the first stage distance-restrained molecular mechanics DUPLEX calculations were used as starting structures for the second stage intensity refinements using the *X-PLOR* program (*31*). In this second stage, we performed molecular dynamics/simulated annealing calculations guided by the combination of the experimental NOESY intensities and NOE distance restraints. The pseudoenergy function included two types of restraints: (1) intensity restraints for nonexchangeable protons were imposed as square-well potentials with an exponent of 2 in the penalty function, an isotropic correlation time of 5 ns, anisotropic bounds estimates of 10%, and a force constant of 50 kcal mol^{-1} $Å^2$, (2) the distance restraints for nonexchangeable protons were retained through our protocol as square-well potentials with uniform 20% estimation of errors and 30 kcal mol^{-1} $Å^2$ force constant. A 4.5 Å cutoff was imposed for computing relaxation pathways, and the dynamics was carried out with a tolerance of 0.03 Å.

The relaxation matrix was set up for the nonexchangeable protons with the exchangeable imino, amino, and hydroxyl protons exchanged for deuterons. A total of 828 nonexchangeable intensity restraints from the NOESY data sets in D_2O (207 intensities per mixing time at 50 ms, 100, 150, and 200 ms) and 207 nonexchangeable distance restraints were included in the calculations. Dihedral angle restraints (corresponding to B-DNA) were included with a very low weight of 5 kcal rad^{-2} and restricted to residues that are two pairs away from the [AF]dG adduct site.

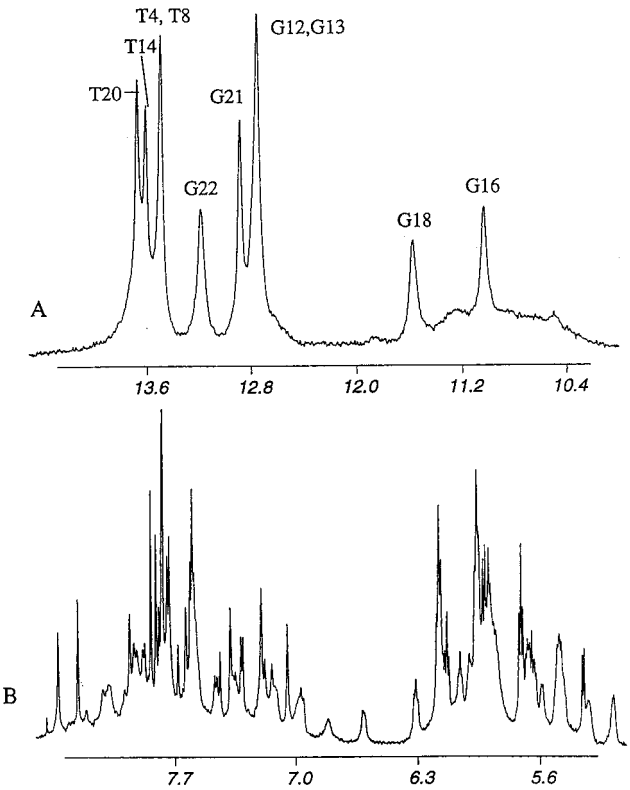

FIGURE 2: (A) Imino proton spectrum (10.2−14.5 ppm) of the [AP]-dG·dA 11-mer duplex in H_2O buffer at 1 °C and (B) nonexchangeable proton spectrum (5.0−8.5 ppm) of the same adduct duplex in D_2O buffer at 25 °C. The buffer was 0.1 M NaCl, 10 mM phosphate, 0.1 mM EDTA, at pH 7.0. The imino proton assignments are shown over the resonances in the spectrum in A.

Six relaxation matrix trials were performed for each of the two DUPLEX-based starting structures. During each run, the starting structure was heated to 1000 °K through the assignment of an arbitrary Maxwell−Boltzmann velocity distribution corresponding to a temperature of 1000 °K. Then, after 2.4 ps dynamics evolution at that temperature, the system was gradually cooled to 300 °K during 7.2 ps with the "heat bath" method and equilibrated at 300 °K for 2.4 ps. After equilibration, the coordinates were subjected to energy minimization to a gradient of 0.1 kcal mol^{-1} $Å^{-1}$.

RESULTS

Exchangeable Nucleic Acid Protons. The exchangeable proton NMR spectrum (10.2−14.5 ppm) of the [AP]dG·dA 11-mer duplex in H_2O buffer solution, pH 7.0, at 1 °C is plotted in Figure 2A. Six well-resolved resonances are observed between 12.5 and 14.0 ppm together with two somewhat broadened and upfield shifted resonances at 11.6 and 11.0 ppm. These imino protons have been assigned following analysis of the NOESY spectrum of the adduct duplex in H_2O buffer based on established assignment procedures (reviewed in *28*).

The expanded NOESY (150 ms mixing time) contour plot of the symmetrical 10.5−14.0 ppm imino proton region of

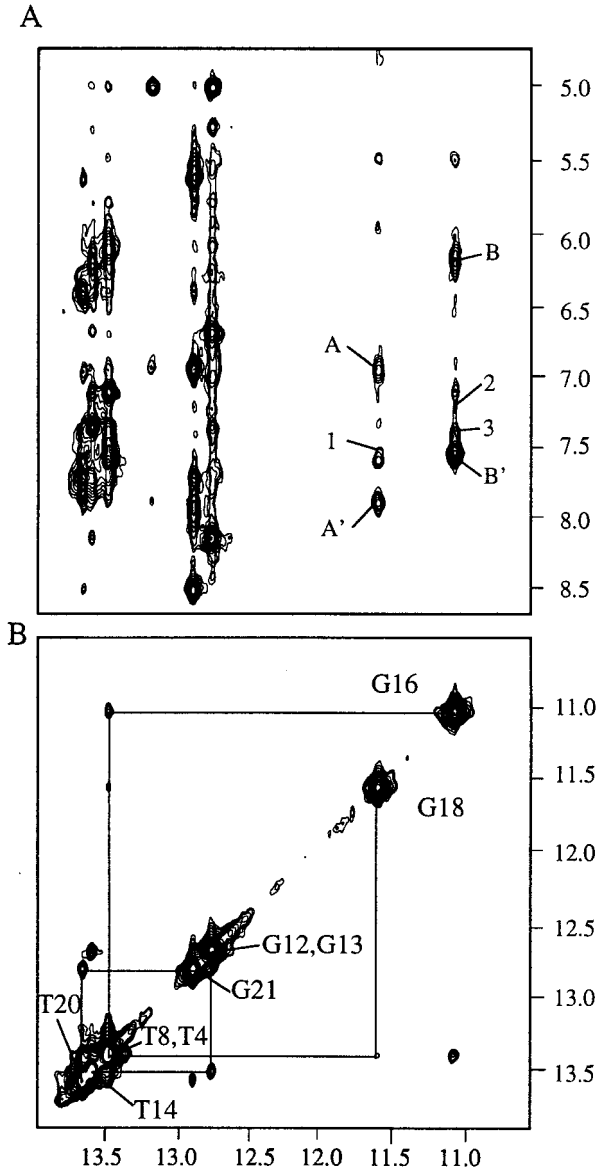

FIGURE 3: Expanded NOESY (150 ms mixing time) contour plots of the [AP]dG·dA 11-mer duplex in H_2O buffer at 1 °C. (A) NOE connectivities between the imino protons (10.5−14.0 ppm) and the base and amino proton regions (4.8−8.7 ppm). The NOE cross-peaks involving the imino protons are labeled in the figure as follows: A,A′, dG18(NH1)−dC5(NH_2-4b,e); B,B′, dG16(NH1)−dC7(NH_2-4b,e). The intermolecular carcinogen−DNA NOE cross-peaks from 1 to 3 are assigned as follows: 1, G18(NH1)−AP(H3); 2, G16(NH1)−AP(H7); 3, G16(NH1)−AP(H9). (B) NOE connectivities in the symmetrical (10.5−14.0 ppm) region. The imino proton assignments are labeled along the diagonal. The lines trace the NOE connectivities where possible between adjacent base pairs starting at dG21 toward one end of the helix and proceeding to dG12 toward the other end of the helix.

the [AP]dG·dA 11-mer duplex is plotted in Figure 3B. The connectivities between imino protons on adjacent base pairs can be traced from the dC11·dG12 pair located at one end of the helix to the dC2·dG21 pair located toward the opposite end of the duplex except that no connectivity is observed between the two upfield-shifted imino protons of dG16 and dG18 in the adduct duplex. The NOE connectivities between the imino protons (10.5−14.0 ppm) and the base/amino protons (4.8−8.6 ppm) are plotted in the corresponding expanded NOESY contour plot of the adduct duplex in Figure 3A. The observed NOE patterns establish Watson−Crick base pairing at all dA·dT pairs (thymine imino to adenine H2 protons) and at all dG·dC pairs (guanine imino to cytosine amino and H5 protons), including the dC5·dG18 and dC7·dG16 base pairs (peaks A, A′ and B, B′, respectively, Figure 3A), which are the nearest residues to the [AP]-dG adduct site. In addition, the two upfield-shifted imino protons of dG16 and dG18 show several cross-peaks to aminopyrene protons (peaks 1 to 3, Figure 3A) in the [AP]-dG·dA 11-mer duplex.

We do not detect the imino proton of the [AP]dG6 adduct in the exchangeable proton spectrum of the [AP]dG·dA 11-mer duplex (Figure 2A), suggesting that this imino proton is not involved in base pairing with dA17 positioned opposite it and is most likely exchanging rapidly with water.

The exchangeable imino and amino proton chemical shifts for the central d(C5−[AP]G6−C7)·d(G16−A17−G18) segment of the [AP]dG·dA 11mer duplex at 1 °C are listed in Table 1 and for the entire adduct duplex in Table S1 (Supporting Information).

Nonexchangeable Nucleic Acid Protons. The base and sugar H1′ nonexchangeable proton spectrum (5.1−8.5 ppm) of the [AP]dG·dA 11-mer duplex in D_2O buffer, pH 7.0 at 25 °C, is plotted in Figure 2B. We observe narrow and well-resolved resonances for the majority of the nucleic acid protons, while somewhat broadened resonances are observed for the aminopyrene protons in the adduct duplex. Nonexchangeable proton assignments are based on an analysis of through-space NOESY and through-bond COSY and TOCSY data sets on the adduct duplex in D_2O buffer at 25 °C based on established assignment procedures (reviewed in *28*).

The expanded NOESY (300 ms mixing time) contour plot establishing sequential connectivities between the base protons (6.5−8.5 ppm) and the sugar H1′ and H3′ protons (4.5−6.5 ppm) of the [AP]dG·dA 11-mer duplex in D_2O buffer, pH 7.0 at 25 °C, are plotted in duplicate in Figure 4. The base to sugar H1′ (and H3′) proton connectivities are traced from dA3 to dA9 along the modified strand (Figure 4A) and from dA15 to dA19 along the complementary strand (Figure 4B) in the adduct duplex. The break in the tracing at the dC5−[AP]dG6 step on the modified strand (Figure 4A) is due to the absence of a purine H8 proton following covalent AP modification at the C^8 position of dG6 in the adduct duplex. Several base to sugar H1′ proton connectivities are very weak or missing for the d(G16−A17−G18) segment on the complementary strand positioned opposite the [AP]dG6 lesion site in the adduct duplex. These base and sugar H1′/H3′ proton assignments have been confirmed by cross-checks in other expanded regions of the NOESY contour plot (Figure 5A) as well as from COSY (Figure 5B) and TOCSY contour plots of the adduct duplex. The nonexchangeable nucleic acid base and sugar proton chemical shifts for the d(C5−[AP]G6−C7)·d(G16−A17−G18) segment of the [AP]dG·dA 11-mer duplex are listed in Table 1 and for the entire adduct duplex in Table S1 (Supporting Information). It should be noted that we have been unable to assign an important marker, namely, the H2 proton of dA17 which is positioned opposite to [AP]dG6 in the adduct duplex.

We observe an inversion of the chemical shifts of the sugar H2′ and H2″ protons at the [AP]dG lesion site in the [AP]-dG·dA 11-mer duplex. Thus, the H2′ proton resonates to the low field at 3.77 ppm relative to the H2″ proton that

Table 1: Proton and Phosphorus Chemical Shifts of the d(T4−C5−[AP]G6−C7−T8)/d(A15−G16−A17−G18−A19) of the [AP]dG·dA 11-mer Duplex[a]

	G(NH1)/T(NH3)	C(NH_2-4)	H8/H6	H5/H2/CH_3	H1′	H2′	H2″	H3′	H4′	$^{31}P^b$
dT4	13.43		7.13	1.44	5.84	1.99	2.37	4.86	4.14	−4.32
dC5		7.89,[c] 6.93[d]	6.98	5.50	5.93	1.21	2.18	4.59	4.11	−3.76
[AP]dG6					6.17	3.77	2.57	5.17	4.42	−3.29
dC7		7.52,[c] 6.17[d]	7.87	5.58	6.00	2.15	2.45	4.81	4.32	−4.04
dT8	13.48		7.37	1.54	5.47	2.11	2.39	4.84	4.13	−4.11
dA15			7.94		5.86	2.54	2.67	4.99	4.30	−4.12
dG16	10.99		6.79		5.31	1.78	2.22	4.95		−3.63
dA17			8.10		5.90	2.58	2.76	5.04	4.54	−3.86
dG18	11.53		7.63			2.38	2.38	4.68	4.16	−4.32
dA19			7.92		6.05	2.45	2.76	4.87	4.31	−4.54

[a] All chemical shifts are in ppm. Exchangeable proton chemical shifts at 1 °C. Nonexchangeable proton and phosphorus chemical shifts at 25 °C. [b] ^{31}P chemical shift corresponds to residue *n* in *n*-^{31}P-(*n*+1) step. [c] Hydrogen-bonded amino proton. [d] Exposed amino proton.

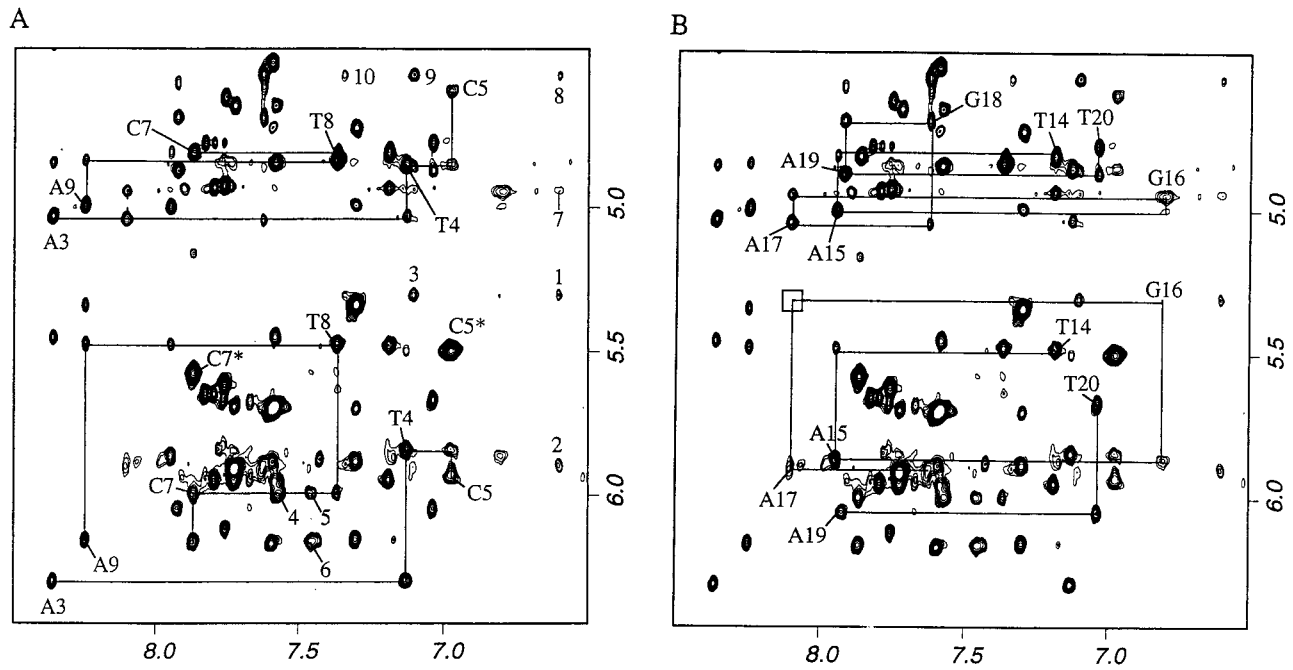

FIGURE 4: Duplicate expanded NOESY (300 ms mixing time) contour plots of the [AP]dG·dA 11-mer duplex in D_2O buffer at 25 °C establishing distance connectivities between the base (purine H8 and pyrimidine H6) protons (6.5−8.6 ppm) and the sugar H1′, H3′ and cytosine H5 protons (4.5−6.5 ppm). The base to sugar H1′ and H3′ proton connectivities are traced in (A) from dT4 to dT8 along the modified strand and in (B) from dT14 to dA19 along the complementary strand. The assignments label base to their own sugar H1′ or H3′ NOEs, while the cytosine H6−H5 NOEs are designated by asterisks. Note that the NOE cross-peak at the dC5−[AP]dG6 is missing in (A) because of the absence of an H8 proton for the [AP]dG6 residue. Note that the base to their own H1′ proton NOEs are weak for dG16 and dA17 and cannot be identified for dG18 in (B). This reflects broadening of some of the base and sugar protons within the d(G16−A17−G18) segment on the partner strand opposite the lesion site in the [AP]dG·dA 11-mer duplex. The intermolecular carcinogen−DNA NOE cross-peaks are assigned as follows: 1, AP(H5)−G16(H1′); 2, AP(H5)−A17(H1′); 3, AP(H6)−G16(H1′); 4, AP(H9)−C7(H1′); 5, AP-(H10)−C7(H1′); 6, AP(H10)−G6(H1′); 7, AP(H5)−G16(H3′); 8, AP(H5)−A17(H4′); 9, AP(H6)−A17(H4′); 10, AP(H7)−A17(H4′). The chemical shift values for the aminopyrene protons in the [AP]dG·dA 11-mer duplex are: AP(H2), 8.07 ppm; AP(H3), 7.59 ppm; AP(H4), 6.95 ppm; AP(H5), 6.61 ppm; AP(H6), 7.10 ppm; AP(H7), 7.34 ppm; AP(H8), 7.56 ppm; AP(H9), 7.58 ppm; AP(H10), 7.46 ppm.

resonates at 2.57 ppm in expanded NOESY (Figure 5A) and COSY (Figure 5B) contour plots of the adduct duplex.

There is no H8 proton for the [AP]dG adduct precluding discrimination of *syn* and *anti* glycosidic torsion angles based on the strength of the NOE between the H8 and H1′ protons (*27*) of this residue in the [AP]dG·dA 11-mer duplex. Previous research on guanine adducts modified at positions other than C^8 have established that *syn* glycosidic torsion angles defined from NOE data are correlated with a large downfield shift in the H2′ proton of the modified guanine in adduct containing duplexes (*32*). The downfield shifted H2′ proton (3.77 ppm) of [AP]dG6 is characteristic of a *syn* glycosic torsion angle at this position in the [AP]dG·dA 11-mer duplex.

Aminopyrene Protons. The nonexchangeable aminopyrene protons were assigned based on the analysis of through-space (NOESY) and through-bond (COSY and TOCSY) data sets of the [AP]dG·dA 11-mer duplex in D_2O buffer, pH 7.0 at 25 °C. The nonexchangeable aminopyrene protons can be traced and assigned as outlined previously for the corresponding [AP]dG·dC 11-mer duplex (*20*), and their values are listed in the caption to Figure 4. The nonexchangeable aminopyrene proton chemical shifts (resonating between 6.5 and 8.1 ppm) exhibit similar patterns in the [AP]dG·dA 11-mer (present study) and [AP]dG·dC 11-mer (*20*) duplexes (Figure S1, Supplemenatry material).

We have also been unable to identify the NH proton involved in the covalent linkage of the aminopyrene and

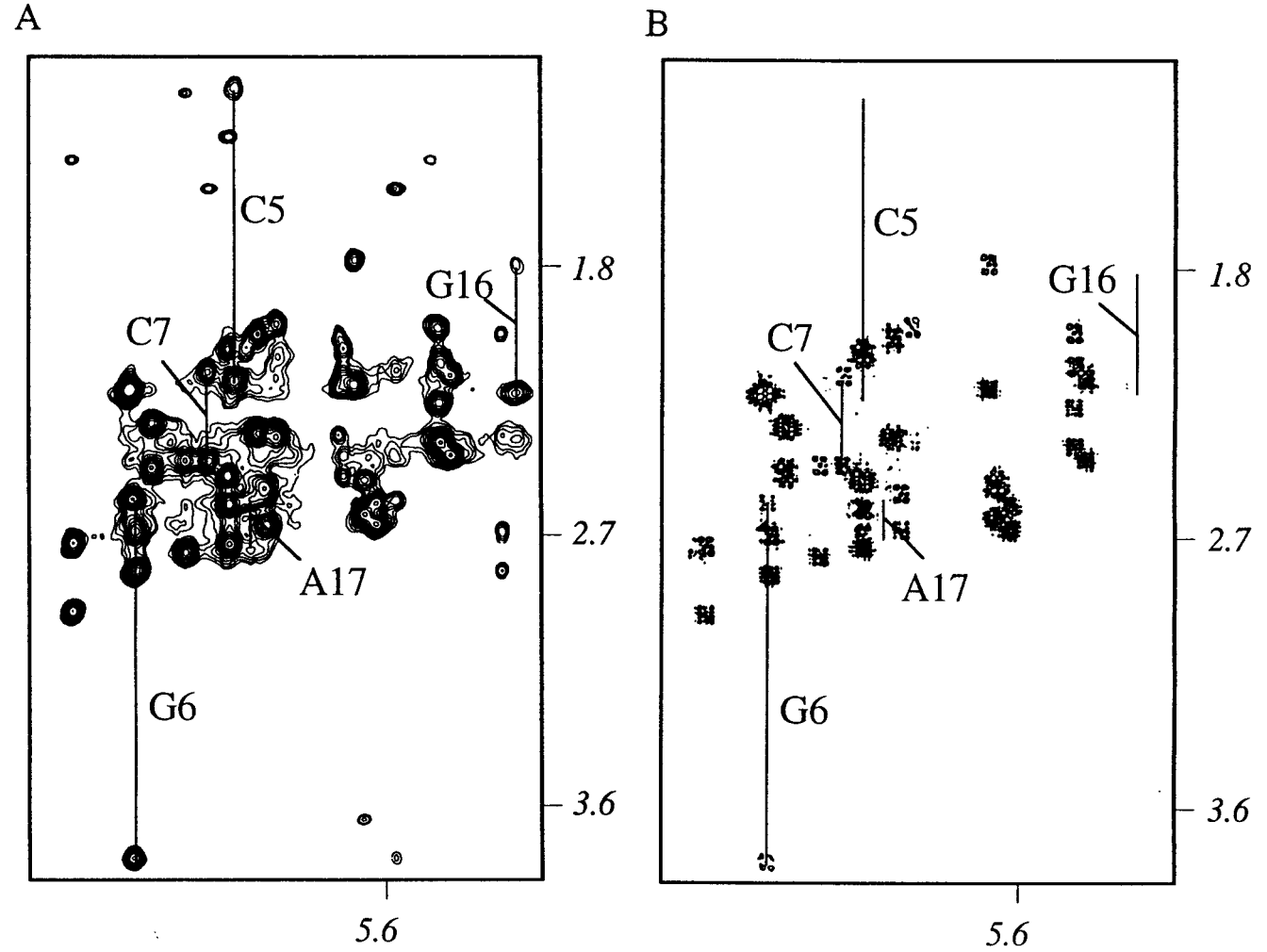

FIGURE 5: (A) An expanded NOESY (200 ms mixing time) contour plot of the [AP]dG·dA 11-mer duplex in D_2O buffer at 25 °C showing NOEs between the sugar H1′ protons (5.2−6.4 ppm) and H2′, H2″ protons (1.1−3.9 ppm). (B) An expanded phase sensitive COSY contour plot of the [AP]dG·dA 11-mer duplex in D_2O buffer at 25 °C establishing coupling connectivities between the H1′ protons (5.2−6.4 ppm) and H2′, H2″ protons (1.1−3.9 ppm). In both (A) and (B) the H2′ and H2″ protons of dC5, [AP]dG6, dC7, dG16, dA17, and dG18 are connected by lines and labeled. The H2′ protons resonate upfield of the H2″ protons for the majority of these residues except for [AP]dG6 where the H2″ proton resonates upfield of the H2′ proton. Note the large downfield shift of the H2′ proton of [AP]dG6 at 3.77 ppm.

Table 2: Intermolecular NOEs between Aminopyrene Protons and DNA Protons

AP protons	DNA protons with NOEs to AP protons[a]
AP(H3)	G18(NH1)*vw*
AP(H5)	G16(H1′)*w*; G16(H2″)*m*; G16(H3′)*vw*; A17(H1′)*w*; A17(H4′)*vw*; G18(H8)*w*
AP(H6)	G16(H1′)*w*; G16(H2′)*w*; G16(H2″)*m*; A17(H4′)*m*; G18(H8)*w*
AP(H7)	G16(NH1)*w*; A17(H4′)*vw*
AP(H9)	C7(H1′)*m*; G16(NH1)*w*
AP(H10)	G6(H1′)*m*; C7(H6)*m*; C7(H1′)*m*

[a] The symbols *m*, *w*, and *vw* stand for medium, weak, and very weak NOEs, respectively.

modified guanine rings in the spectrum of the [AP]dG·dA 11-mer duplex at either pH 7.0 or pH 5.0 in H_2O buffer solution.

Carcinogen−DNA NOEs. The intermolecular NOEs between the aminopyrene ring and DNA protons that have been identified in the NOESY spectra of the [AP]dG·dA 11mer duplex are listed in Table 2. Some of these intermolecular AP−DNA NOE cross-peaks are labeled by numbers in the expanded NOESY plots of the exchangeable protons of the adduct duplex in H_2O solution (Figure 3) and nonexchangeable protons in D_2O solution (Figure 4) with their assignments listed in the figure captions.

The observed NOEs between the H3, H7, and H9 aminopyrene protons and the dG16 and dG18 imino protons position the aminopyrene between the dC5·dG18 and dC7·dG16 base pairs in the adduct duplex. The NOEs between the H5, H6, and H7 aminopyrene protons at the [AP]dG6 adduct site, the H1′, H2″, and H3′ sugar protons of dG16, and the H1′ and H4′ sugar protons of dA17 establish that the aminopyrene ring edge furthest from the covalent linkage site is positioned near the sugar protons of dG16 and dA17 on the unmodified strand of the [AP]dG·dA 11-mer duplex. By contrast, the H9 and H10 aminopyrene protons that are close to the covalent linkage site show NOEs to the H1′ sugar protons of dG6 and dC7 of the modified strand in the adduct duplex.

Carbon Spectra. The expanded contour plot of a natural abundance $^1H-^{13}C$ HMQC correlation experiment that correlates the H1′ and C1′ chemical shifts of individual residues for the [AP]dG·dA 11-mer duplex in D_2O buffer at 25 °C is plotted in Figure 6A. The carbon resonances are assigned on the basis of the known H1′ proton assignments

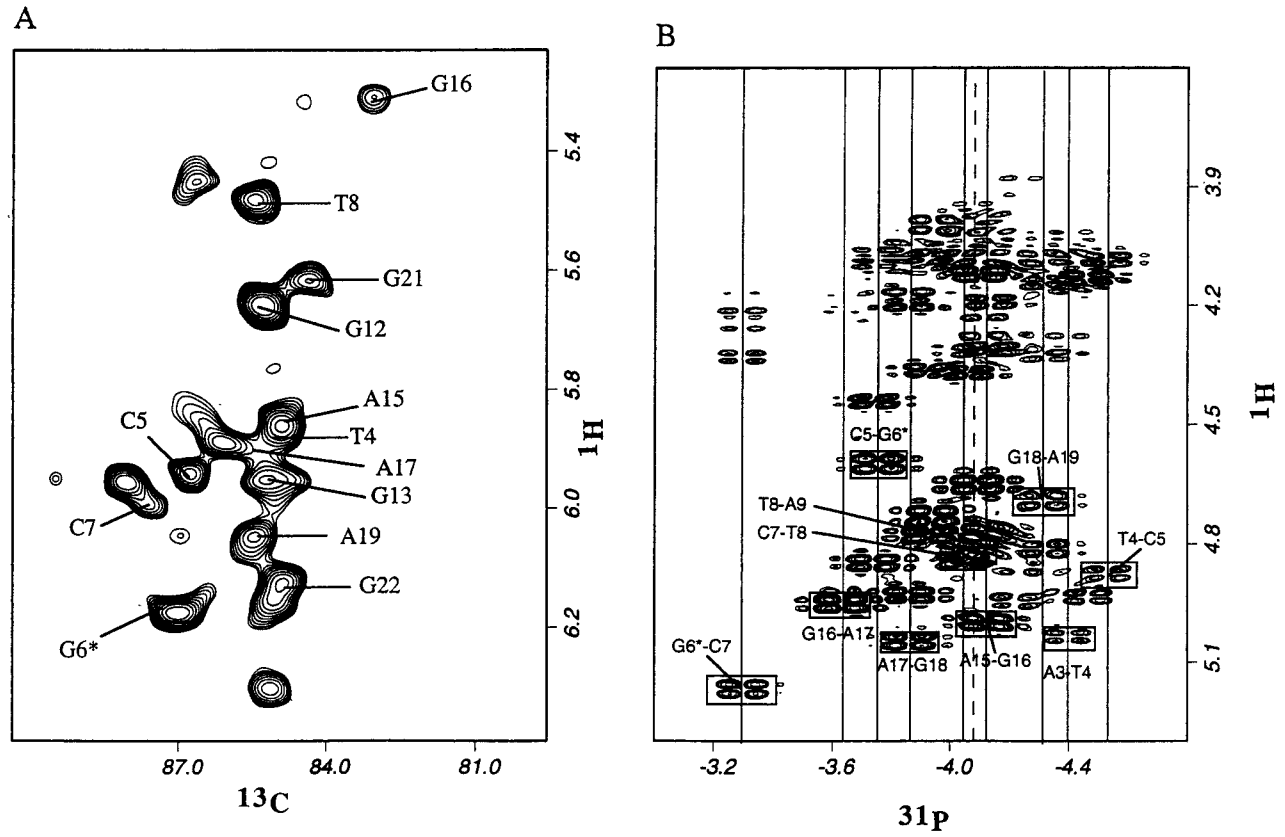

FIGURE 6: (A) An expanded contour plot of $^{1}H/^{13}C$ heteronuclear multiple-quantum coherence (HMQC) experiment on the [AP]dG·dA 11-mer duplex in D_2O buffer at 25 °C. The C1′ assignments are marked for residues in the d(T4−C5−[AP]G6−C7−T8)·d(A15−G16−A17−G18−A19) segment. (B) An expanded contour plot of the proton-detected phosphorus−proton heteronuclear correlation experiment on the [AP]dG·dA 11-mer duplex in D_2O buffer at 25 °C. The phosphorus assignments are listed for steps centered about the lesion site. The correlation cross-peaks between the phosphorus and its 5′-flanking sugar H3′ protons are boxed.

in the [AP]dG·dA 11-mer duplex. The C1′ chemical shift assignments for residues in the d(C5−[AP]G6−C7)·d(G16−A17−G18) segment in the adduct duplex are labeled in Figure 6A. It is noted that the 86.7 ppm ^{13}C chemical shift of the C1′ carbon of [AP]dG6 is downfield shifted relative to other assignable C1′ carbons of guanine residues in this segment of the adduct duplex (Figure 6A). It has been previously established that sugar C1′ carbon chemical shifts of DNA residues adopting *syn* glycosidic torsion angles can downfield shift by up to 5 ppm when these DNA residues retain C2′-*endo* sugar pucker geometries (*33*, *34*). We have detected a relatively strong coupling cross-peak between the H1′ (6.17 ppm) and H2′ (3.77 ppm) protons of [AP]dG6 (Figure 4B) placing this sugar within the C2′-*endo* range.

Phosphorus Spectra. The proton-decoupled phosphorus spectrum of the [AP]dG·dA 11-mer duplex has been recorded in D_2O buffer at 25 °C. The phosphorus resonances are dispersed over a 1.4 ppm chemical shift range with several resonances shifted to lower field relative to the −3.8 to −4.5 ppm spectral region. The phosphorus resonances have been assigned from an analysis of the proton detected phosphorus−proton heteronuclear correlation experiment with the expanded contour plot shown in Figure 6B and their values listed for the central segment in Table 1 and for the entire molecule in Table S1. The three- and four-bond proton−phosphorus vicinal couplings permit the correlation of the phosphorus resonances with their 5′-linked H3′ proton and the 3′-linked H4′ and H5′,5″ protons. The phosphorus chemical shifts for the d[AP]G6−dC7 (−3.29 ppm), dG16−dA17 (−3.63 ppm), and dC5−d[AP]G6 (−3.76 ppm) steps are shifted to the lower field of the −3.8 to −4.5 ppm unperturbed phosphodiester backbone chemical shift range.

Distance-Restrained Molecular Mechanics Refinement. The search strategy employed began with a B-DNA (*35*) central d(T4−C5−[AP]G6−C7−T8)·d(A15−G16−A17−G18−A19) base pair segment of the [AP]dG·dA 11-mer duplex. The computations were guided by the intramolecular DNA and intermolecular AP−DNA distance restraints within this segment of the adduct duplex. The AP−DNA orientation space was searched with 16 energy minimization trials in which the linkage torsion angles α′ ([AP]dG6(N^9)−[AP]dG6-(C^8)−[AP](N)−[AP](C^1)) and β′ ([AP]dG6(C^8)−[AP](N)−[AP](C^1)−[AP](C^{10A})) were each started at 0°, 90°, 180°, and 270° in all combinations, and the glycosidic torsion angle χ for [AP]dG6 residue was started at *syn* (60°) consistent with the NMR data. Searching orientation space at 90° intervals of α′ and β′ is a robust procedure for locating all the important potential energy wells because our minimization protocol permits torsion angle variations of up to 100° in each minimization step (*29*). Consequently, energy minima in each quadrant of α′ and β′ are accessible and the reduced variable domain of torsion angle space greatly enhances the likelihood of finding the important structures. In these trials, the DUPLEX hydrogen-bond penalty function (*29*) for Watson−Crick base pairing was utilized at all base pairs, except the [AP]dG6·dA17 site since the NMR data indicated these pairing alignments.

The 16 computed structures produced five structures with low energies and goodness-of-fit indices that fell into two families. The AP ring is intercalated between flanking dG·dC base pairs in both families of structures. In one family with three-members, the dG6 was 3′-directed (Figure S2A, Supporting Information), while it was 5′-directed in the second family that contains two members (Figure S2B, Supporting Information). The energies and goodness-of-fit indices for these two families are listed in Table S2 (Supporting Information). One member of each family with lowest combined goodness-of-fit indices was embedded into an energy minimized B-form 11-mer and reminimized with all restraints. These two structures were employed as starting points for the subsequent relaxation matrix refinement computations.

Relaxation Matrix Refinement. A total of 21 structures corresponding to the 5′-directed dG6 in the [AP]dG·dA 11-mer duplex were obtained following intensity refinement from the two starting structures provided by the molecular mechanics calculations. By contrast, only 3 structures corresponding to the 3′-directed dG6 were obtained following intensity refinement. The majority of the structural features are the same for the 5′-directed and 3′-directed conformations, which differ primarily at the α' and β' angles of the aminopyrene linkage site.

An ensemble of nine intensity-refined structures corresponding to the 5′-directed conformation demonstrated an improved correspondence with experimental intensity and distance restraint data sets compared to the 5′-directed structure obtained from the first stage molecular mechanics calculations. The number of NOE distances violated by more than 0.2 Å decreased from 40 to 8 [with only 1 to 2 violations in the central 5-mer d(T4−C5−[AP]G6−C7−T8)·d(A15−G16−A17−G18−A19) segment with respect to different structures in the ensemble], and the NMR *R*-factor ($R_{1/6}$) improved from a value of 8.6% after distance refinement to 3.5% after intensity refinement. The experimental distance bounds of the [AP]dG·dA 11-mer duplex are compared with those observed after relaxation matrix refinement in Table S3 (Supporting Information).

The pairwise rmsd of the nine intensity refined structures in the set is 1.71 ± 0.34 Å for the heavy atoms of the entire adduct duplex and 1.26 ± 0.18 Å for the heavy atoms of the central d(T4−C5−[AP]G6−C7−T8)·d(A15−G16−A17−G18−A19) segment (Table 3). The structures exhibit good stereochemistry with reasonable rmsd values for bond length, bond angle, and improper dihedral angle violations (Table 3).

A view of six superpositioned structures from the set of nine structures of the d(T4−C5−[AP]G6−C7−T8)·d(A15−G16−A17−G18−A19) segment of the [AP]dG·dA 11-mer duplex is plotted in Figure 7A. The corresponding view looking down the helix axis of the central dC5−[AP]G6−C7)·d(G16−A17−G18) segment of the adduct duplex is plotted in Figure 7B. The refined structures of the central segment of the adduct duplex have several features in common and some segments that are less well-defined. Both the aminopyrene ring and the modified guanine ring of [AP]dG6 adduct site are well-defined in contrast to dA17 positioned opposite it, which is poorly defined among the ensemble of refined structures (Figure 7A). Further, the Watson−Crick dC7·dG16 base pair is better defined than the Watson−Crick dC5·dG18 base pair that flank the intercalated aminopyrene ring in the structures of the adduct duplex (Figure 7A).

Table 3: NMR Refinement Statistics for the [AP]dG·dA 11-mer Duplex

NMR distance restraints	
entire 11-mer adduct duplex	207
central 5-mer region[a]	95
carcinogen-DNA restraints	19
NMR intensity restraints	
entire 11-mer adduct duplex	828 (4 mixing times)
central 5-mer region[a]	380 (4 mixing times)
structure statistics	
NMR *R*-factor ($R_{1/6}$)	0.035 ± 0.001
rmsd of NOE violations	0.068 ± 0.006
number of NOE violations >0.2 Å in the entire adduct duplex	8.2 ± 1.8
number of NOE violations >0.2 Å in the central 5-mer region[a]	1.2 ± 1.1
deviations from the ideal geometry	
bond length (Å)	0.011 ± 0.001
bond angle (deg)	2.97 ± 0.12
impropers (deg)	0.46 ± 0.13
pairwise rmsd (Å) among the nine refined structures (heavy atoms only)	
entire 11-mer adduct duplex	1.71 ± 0.34
central 5-mer region[a]	1.26 ± 0.18

[a] The d(T4−C5−[AP]G6−C7−T8)·d(A15−G16−A17−G18−A19) segment.

Solution Structures. The same two views as in Figures 7A and 7B for the central d(C5−[AP]G6−C7)·d(G16−C17−G18) segment in one representative refined structure of the [AP]dG·dA 11-mer duplex are shown in Figures 8A and 8B, respectively. The covalently linked aminopyrene ring intercalates between Watson−Crick dC5·dG18 and dC7·dG16 base pairs by displacing the modified guanine ring of the *syn* [AP]dG6 residue and the adjacent dA17 residue into the major groove (Figure 8A). The dA17 base, which is less well-defined, is not looped out of the helix but rather forms an in-plane base platform with dG18 in several of the refined structures of the complex. The aminopyrene ring resides in a hydrophobic pocket generated by the base rings of dC5, dC7, dG16, dA17, and dG18 in the adduct duplex. The dC7·dG16 base pair is positioned below the center of the aminopyrenyl ring with the purine ring of dG16 overlapping significantly with the intercalated aminopyreneyl ring (Figure 8B). By contrast, the dC5·dG18 base pair only partially overlaps with the intercalated aminopyrenyl ring (Figure 8B). In addition, there is stacking between the dC5 base and the looped out modified guanine of [AP]dG6 (Figure 8A).

The carcinogen-base linkage site for the [AP]dG6 residue is defined by the torsion angles α' ([AP]dG6(N^9)−[AP]dG6-(C^8)−[AP](N)−[AP](C^1)) = 148.6 ± 9.4 and β' ([AP]dG6-(C^8)−[AP](N)−[AP](C^1)−[AP](C^{10A})) = 213.8 ± 8.5°, with a resultant tilt of the looped out modified dG6 ring toward the 5′ end (Figure 8A). The *syn* glycosidic torsion angle at the [AP]dG6 residue spans the range χ(O4′−C1′−N9−C4) = 76° ± 6°. The deoxyribose conformation at dG18 is C3′-*endo* (P = 10° ± 6°) among the refined structures of the adduct duplex.

A stereoview of one intensity-refined structure of the entire [AP]dG·dA 11-mer duplex is shown in Figure 9.

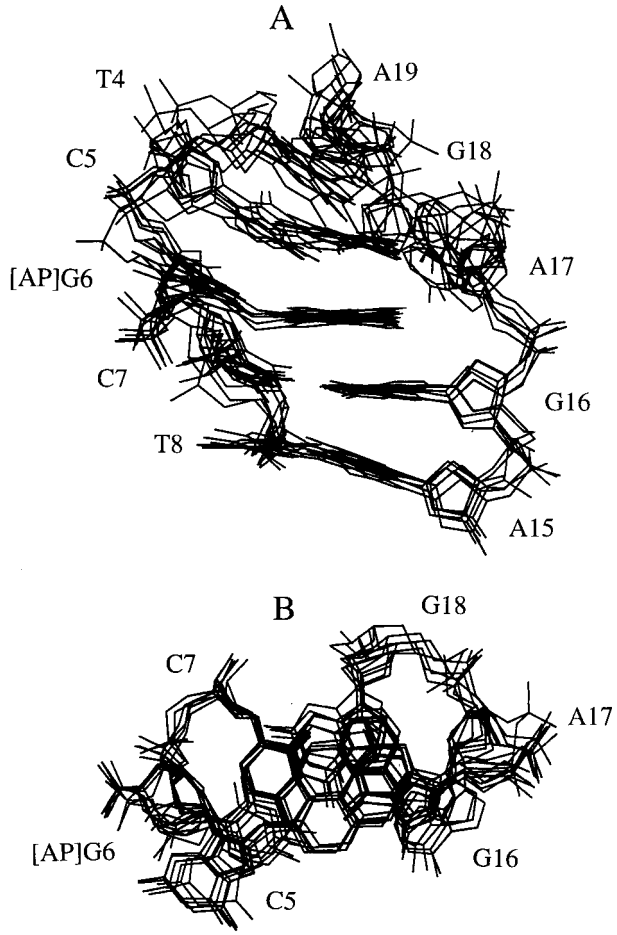

FIGURE 7: (A) The superposition of the d(T4−C5−[AP]G6−C7−T8)·d(A15−G16−A17−G18−A19) segments of six relaxation matrix refined structures of the [AP]dG·dA 11-mer duplex. View looking into the major groove and normal to the helix axis. (B) The superposition of the d(C5−[AP]G6−C7)·d(G16−A17−G18) segments of six relaxation matrix refined structures of the [AP]-dG·dA 11-mer duplex. View looking down the helix axis.

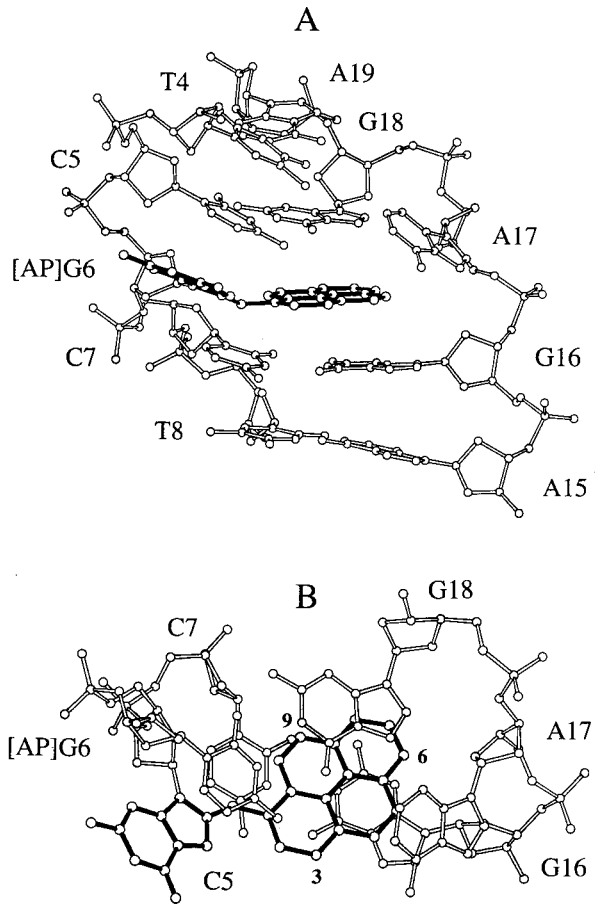

FIGURE 8: A representative relaxation matrix refined structure of the [AP]dG·dA 11-mer duplex. (A) View looking into the major groove and normal to the helix axis of the central d(T4−C5−[AP]-G6−C7−T8)·d(A15−G16−A17−G18−A19) segment. The [AP]-dG6 ring system is shown in darkened bonds and is intercalated between the dC5·dG18 and dC7·dG16 base pairs. The modified dG6 base is displaced into the major groove and directed toward the 5′-end of the modified strand. (B) View looking down the helix axis for the d(C5−[AP]G6−C7)·d(G16−A17−G18) segment. Figures were prepared using Molscript VI.1 (*52*).

DISCUSSION

Spectral Quality and Information Content. The majority of the exchangeable and nonexchangeable protons exhibit narrow and well-resolved spectra facilitating the assignment of the resonances in the [AP]dG·dA 11-mer duplex. The broadening of several protons associated with the d(G16−A17−G18) segment opposite the [AP]dG6 adduct site has resulted in weak NOE (Figure 4) and weak or absent coupling (Figure 5B) cross-peaks for protons originating in this segment of the adduct duplex.

Chemical Shift Patterns in the [AP]dG·dA 11-mer. The intercalation of the aromatic aminopyrenyl ring of the [AP]-dG6 between dC5·dG18 and dC7·dG16 base pairs is strongly supported by the observed experimental chemical shift patterns for the adduct duplex. Thus, the imino protons of dG16 and dG18 undergo upfield shifts of ∼1.2 ppm, while the amino protons of dC7 and dC5 undergo upfield shifts of ∼0.4−0.5 ppm on proceeding from the unmodified control 11-mer duplex to the [AP]dG·dA 11-mer duplex. These shifts must reflect upfield ring current contributions from the aminopyrene ring that is intercalated between the dC5·dG18 and dC7·dG16 base pairs in all the refined structures of the adduct duplex.

The stacking of the dC5 residue over the purine ring of the looped out modified guanine of [AP]dG6 is reflected in the upfield shifts for the H2′ (1.21 ppm) and H2″ (2.18 ppm) sugar protons of dC5 in the spectrum of the adduct duplex.

Comparison of [AP]dG·dC 11-mer and [AP]dG·dA 11-mer Duplexes. A comparison of the solution structures of the [AP]dG·dC 11-mer (*20*) (Figure S3, Supporting Information) and the [AP]dG·dA 11-mer (present study) (Figure 8A) duplexes establishes common structural features as well as some differences centered about the adduct site. Thus, the aminopyrene ring intercalates between intact base pairs with the modified guanine in a *syn* alignment displaced into the major groove in both adduct duplexes.

This base displacement architecture appears to be achieved either through alignment of the modified guanine toward the 3′-direction of the modified strand as observed for the [AP]-dG·dC 11-mer duplex (*20*) (Figure S3, Supporting Information) or toward the 5′-direction of the modified strand as observed for the [AP]dG·dA 11-mer duplex (present study) (Figure 8A). It is unfortunate that we have been unable to identify the NH proton involved in the covalent linkage of the aminopyrene and modified guanine rings in the adduct

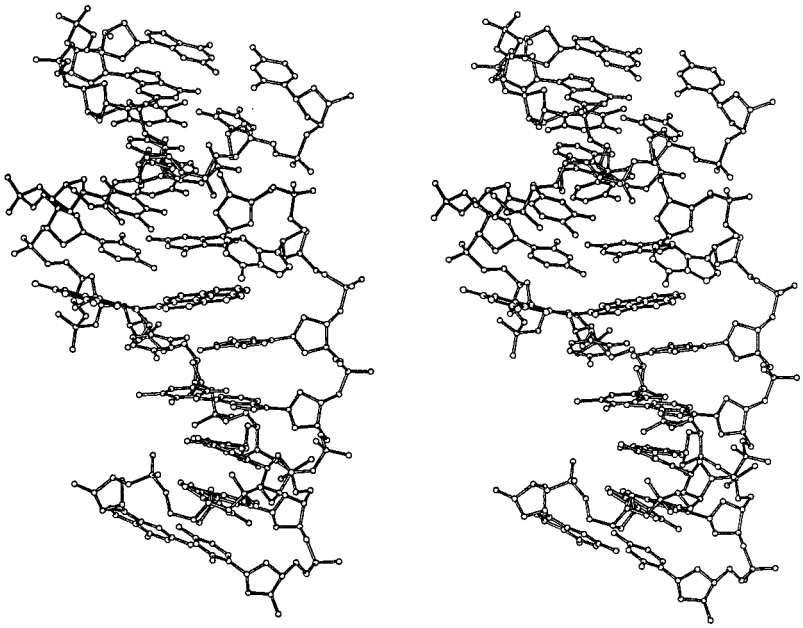

FIGURE 9: A stereoview of a representative relaxation matrix refined structure of the entire [AP]dG·dA 11-mer duplex.

duplex. This proton would be directed toward and show NOEs to the dC5·dG18 base pair when the modified guanine of [AP]dG is directed toward the 3′-direction, while it would be directed toward and show NOEs to the dC7·dG16 base pair when the modified guanine of [AP]dG is directed toward the 5′-direction. The torsion angles linking the modified deoxy guanosine to the pyrenyl ring adopt values of $\alpha' = 209°$ and $\beta' = 141°$ for the [AP]dG·dC 11-mer duplex (*20*) and $\alpha' = 149°$ and $\beta' = 214°$ for the [AP]dG·dA 11-mer duplex (present study).

The least well-defined segment of the [AP]dG·dC 11-mer (*20*) and [AP]dG·dA 11-mer (present study) duplexes concerns the bases positioned opposite the adduct site. This is in part due to the broadening of proton resonances of residues in the d(G16−C/A17−G18) trinucleotide segment positioned opposite the adduct site in both duplexes. The pyrimidine ring of dC17 is displaced into the major groove and does not interact with either the [AP]dG adduct or residues centered about the adduct site in the [AP]dG·dC 11-mer duplex (*20*). By contrast, the purine ring of dA17 is positioned closer to the helix axis and, in some of the refined structures, participates in an in-plane base platform (*36*, *37*) at the dA17−dG18 step in the [AP]dG·dA 11-mer duplex (Figure 8A). Such an in-plane stacking alignment contributes to formation of a hydrophobic core involving the dC5, dC7, dG16, dA17, and dG18 residues surrounding the intercalated aminopyrenyl aromatic ring system in the adduct duplex.

Comparison of [AP]dG·dA 11-mer and [AF]dG·dA 11-mer Duplexes. The solution structure of of the [AP]dG·dA 11-mer duplex reported in this study can be compared with the solution structure reported previously for the [AF]dG·dA 11-mer duplex (*21*) in the same sequence context. The aminopyrene AP ring is larger than the aminofluorene AF ring, and this has dramatic consequences relating to the alignment of both the adduct and the dA positioned opposite it in the [AP]dG·dA 11-mer and [AF]dG·dA 11-mer duplexes.

The base displacement-intercalation structure at the adduct site (Figure 8A) observed for the [AP]dG·dA 11-mer duplex reported in this study is distinctly different from the corresponding structure at the adduct site in the [AF]dG·dA 11-mer duplex (*21*). Both the modified dG and the dA positioned opposite it are stacked into the helix with the aminofluorenyl ring sandwiched between the walls of the minor groove and directed toward the partner strand in the solution structure of the [AF]dG·dA 11-mer duplex (Figure 10). The torsion angles linking the modified guanine to the aminopyrenyl ring adopt values of $\alpha' = 149°$ and $\beta' = 214°$ for the [AP]dG·dA 11-mer duplex (present study), while those linking the modified guanine ring to the aminofluorenyl ring adopt values of $\alpha' = 208°$ and $\beta' = 317°$ for the [AF]-dG·dA 11-mer duplex (*21*).

It, therefore, appears that the bulkier aminopyrenyl ring in the [AP]dG·dA 11-mer duplex cannot be accommodated edge-wise within the walls of the minor groove without significant exposure of its aromatic surface to solvent in contrast to adoption of this architecture by the smaller aminofluorenyl ring in the [AF]dG·dA 11-mer duplex. Hence, the aminopyrenyl ring prefers to intercalate into the helix maximally burying its aromatic surface and achieves this through base displacement of its modified guanine into the major groove in the [AP]dG·dA 11-mer duplex.

Biological Significance. Frameshift mutagenesis has long been hypothesized to occur as a result of misaligned structures in appropriate sequence contexts, which can be stabilized by intercalation of planar aromatic moieties (*38*−*40*). More recently, the concept has been developed further and applied to unmodified DNA (*41*, *42*) and carcinogen-modified DNA (*43*−*47*). The essential idea involves stalling of a polymerase in the vicinity of the damaged base, which permits time for a rearrangement in which an unopposed bulge can form. It is not surprising that [AP]dG, a lesion that predominantly induces frameshift mutagenesis in bacteria, does not maintain hydrogen bonding with either dC (*20*) or dA (present study) in the complementary strand. This must reflect displacement of the modified dG into the major groove, with intercalation of the aminopyrene residue into the helix, but with little distortion beyond the lesion site and

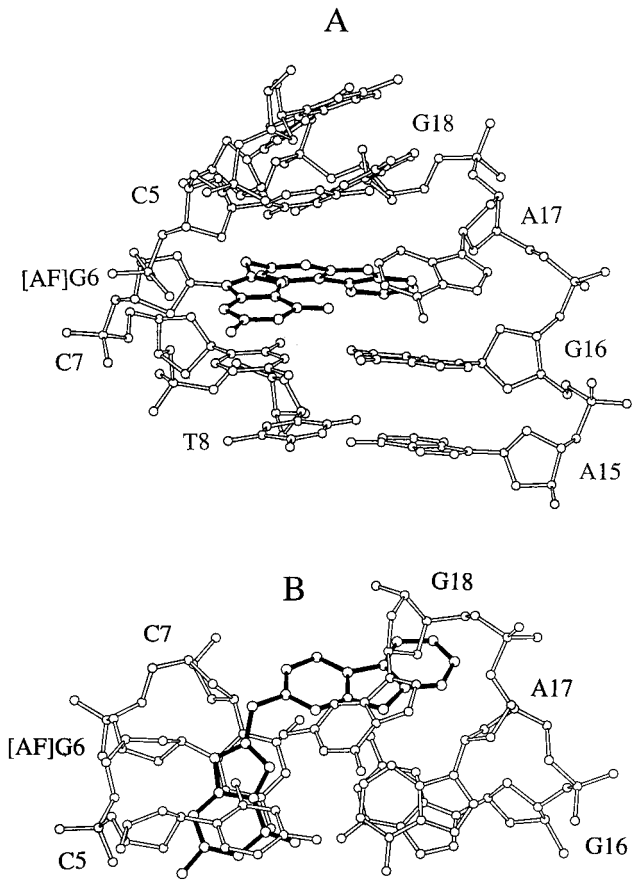

FIGURE 10: A representative distance-restrained molecular mechanics DUPLEX program refined structure of the [AF]dG·dA 11-mer duplex. (A) View looking into the major groove and normal to the helix axis of the central d(T4−C5−[AF]G6−C7−T8)·d(A15−G16−A17−G18−A19) segment. The [AF]dG6 ring system is shown in darkened bonds with the modified guanine and dA17 stacked into the helix between the dC5·dG18 and dC7·dG16 base pairs and the aminofluorene ring positioned in the minor groove and directed toward the partner strand. (B) View looking down the helix axis for the d(C5−[AF]G6−C7)·d(G16−A17−G18) segment. Figures were prepared using Molscript VI.1 (*52*).

with flanking base pairs intact. If such non-hydrogen-bonded duplexes featuring base displacement with carcinogen intercalation occurred at a replication fork, irrespective of whether dCMP or dAMP was incorporated opposite the adduct, polymerase stalling might become more probable, with formation of a slipped frameshift intermediate in an appropriate sequence context. Because of the absence of hydrogen bonding interactions, the nucleotide opposite the adduct may also be subject to excision by the proofreading exonuclease of the DNA polymerase. The latter would also cause stalling of the DNA polymerase, which in turn may allow more time for the formation of slipped frameshift intermediates. While translesion synthesis may be induced by the SOS type of inducible proteins, such forced replication would likely result in increased mutagenesis (*16*).

In conclusion, incorporation of dA opposite [AP]dG produces a base-displaced, intercalated structure without hydrogen bonding between the [AP]dG and the opposite mismatched dA. Such a structure, if present at a replication fork, may cause polymerase stalling and formation of a slipped intermediate that could produce frameshift mutations, the most dominant mutagenic consequence of the [AP]dG lesion in bacteria. It is interesting to note that 2-acetylaminofluorene (AAF) modified dG, which also adopts a base-displaced, AAF intercalated conformation (*48*−*50*), also has a very high propensity to cause frameshift mutations (*51*).

Coordinates Deposition. The coordinates of the [AF]dG·dA 11-mer duplex have been deposited in the Protein Data Base, Brookhaven National Laboratory, Upton, New York 11923, (acquisition number: 1axu) from whom copies can be obtained.

SUPPORTING INFORMATION AVAILABLE

Four tables listing the complete exchangeable and non-exchangeable proton chemical shifts, goodness-of-fit data following distance-restrained DUPLEX refinement, comparison of experimental distance restraints with corresponding values in relaxation matrix refined structures and pseudorotation and glycosidic torsion angles for the [AP]-dG·dA 11-mer duplex, and three figures comparing aminopyrene chemical shifts for [AP]dG positioned opposite dC and dA, distance-restrained DUPLEX structures of the central segment of the [AP]dG·dA 11-mer duplex and the central segment of the [AP]dG·dC 11-mer duplex. This material is available free of charge via the Internet at http://pubs.acs.org.

REFERENCES

1. Rosenkranz, H. S., McCoy, E. C., Sanders, D. R., Butler, M., Kiriazides, D. K., and Mermelstein, R. (1980) *Science 209*, 1039−1043.
2. Heflich, R. H., Howard, P. C., and Beland, F. A. (1985) *Mutat. Res. 149*, 25−32.
3. IARC (1989) *Diesel and gasoline engine exhausts and some nitroarenes*. In *IARC Monographs on the Evaluation of Carcinogenic Risk to Humans*, Vol. 39, IARC, Lyon, France.
4. Ohnishi, Y., Kinouchi, T., Manabe, Y., Tsutsui, O., H., Tokiwa, H., and Otofuji, T. (1985) *Nitro compunds in environmental mixtures and foods*. In *Short-Term Genetics Bioassays in the Evaluation of Complex Environmental Mixtures*, Plenum Press, New York.
5. Kinouchi, T., Tsutsui, H., and Ohnishi, Y. (1986) *Mutat. Res. 171*, 105−113.
6. Rosenkranz, H. S., and Mermelstein, R. (1985) *J. Environ. Sci. Health, Part C3*, 221−272.
7. McGregor, W., Maher, V., and McCormick, J. (1994) *Cancer Res. 54*, 4207−4213.
8. Hirose, M., Lee, M.-S., Wang, C. Y., and King, C. M. (1984) *Cancer Res. 44*, 1158−1162.
9. Wislocki, P., Bagan, E., Lu, A., Dooley, K., Fu, P., Han-Hsu, H., Beland, F., and Kadlubar, F. (1986) *Carcinogenesis 7*, 1317−1322.
10. Wei, S.-J. C., Chang, R. L., Wong, C.-Q., Bhachech, N., Cui, X. X., Hennig, E., Yagi, H., Sayer, S. M., Jerina, D. M., Preston, B. D., and Conney, A. H. (1991) *Proc. Natl. Acad. Sci. U.S.A. 88*, 11227−11230.
11. Howard, P. C., Heflich, R. H., Evans, F. E., and Beland, F. A. (1983) *Cancer Res. 43*, 2052−2058.
12. Stanton, C. A., Chow, F. L., Phillips, D. H., Grover, P. L., Garner, R. C., and Martin, C. N. (1985) *Carcinogenesis 6*, 535−538.
13. Stanton, C. A., Garner, R. C., and Martin, C. N. (1988) *Carcinogenesis 9*, 1153−1157.
14. Melchior, W. B. J., Marques, M. M., and Beland, F. A. (1994) *Carcinogenesis 15*, 889−899.
15. Malia, S. A., and Basu, A. K. (1995) *Biochemistry 34*, 96−104.
16. Malia, S. A., Vyas, R. R., and Basu, A. K. (1996) *Biochemistry 35*, 4568−4577.
17. Yang, J. L., Maher, V. M., and McCormick, J. J. (1988) *Mol. Cell. Biol. 8*, 3364−3372.
18. Newton, R. K., Mittelstaedt, R. A., Manjanantha, M. G., and Helfich, R. H. (1992) *Carcinogenesis 13*, 819−825.

19. Napolitano, R. L., Lambert, I. B., and Fuchs, R. P. P. (1997) *Proc. Natl. Acad. Sci. U.S.A.* 94, 5733−5738.
20. Mao, B., Vyas, R. R., Hingerty, B. E., Broyde, S., Basu, A. K., and Patel, D. J. (1996) *Biochemistry 35*, 12659−12670.
21. Norman, D., Abuaf, P., Hingerty, B. E., Live, D., Grunberger, D., Broyde, S., and Patel, D. J. (1989) *Biochemistry 28*, 7462−7476.
22. Vyas, R. R., Nolan, S. J., and Basu, A. K. (1993) *Tetrahedron Lett. 34*, 2247−2250.
23. Nolan, S. J., Vyas, R. R., Hingerty, B. E., Ellis, S., Broyde, S., Shapiro, R., and Basu, A. K. (1996) *Carcinogenesis 17*, 133−144.
24. Marion, D., Ikura, M., Tschudin, R., and Bax, A. (1989) *J. Magn. Reson. 85*, 393−399.
25. Sklenar, V., Miyashiro, H., Zon, G., Miles, H. T., and Bax, A. (1986) *FEBS Lett. 208*, 94−98.
26. Bax, A., and Subramanian, J. (1986) *J. Magn. Reson. 67*, 565−570.
27. Patel, D. J., Kozlowski, S. A., Nordheim, A., and Rich, A. (1982) *Proc. Natl. Acad. Sci. U.S.A. 79*, 1413−1417.
28. van de Ven, F. J., and Hilbers, C. W. (1988) *Eur. J. Biochem. 178*, 1−38.
29. Hingerty, B. E., Figueroa, S., Hayden, T., and Broyde, S. (1989) *Biopolymers 28*, 1195−1222.
30. Taylor, E. R., and Olson, W. K. (1983) *Biopolymers 22*, 2667−2702.
31. Brunger, A. T. (1992) *X-Plor: A system for X-ray Crystallography and NMR*, Yale University Press, New Haven and London.
32. Cosman, M., Hingerty, B. E., Geacintov, N. E., Broyde, S., and Patel, D. J. (1995) *Biochemistry 34*, 15334−15350.
33. Ghose, R., Marino, J. P., Wiberg, K. B., and Prestegard, J. H. (1994) *J. Am. Chem. Soc. 116*, 8827−8828.
34. Greene, K. L., Wang, Y., and Live, D. (1995) *J. Biomol. NMR 5*, 333−338.
35. Arnott, S., Bond, P. J., Selsing, E., and Smith, P. J. (1976) *Nucl. Acids Res. 2*, 2459−2470.
36. Cate, J., Gooding, A., Podell, E., Zhou, K., Golden, B., Kundrot, C., Cech, T., and Doudna, J. (1996) *Science 273*, 1678−1685.
37. Cate, J., Gooding, A., Podell, E., Zhou, K., Golden, B., Szewczak, A., Kundrot, C., Cech, T., and Doudna, J. (1996) *Science 273*, 1696−1699.
38. Streisinger, G., Okada, Y., Emrich, J., Newton, J., Tsugita, A., Terzaghi, E., and Inouye, M. (1966) *Cold Spring Harbor Symp. Quantum Biol. 31*, 77−84.
39. Drake, J. W., and Baltz, R. W. (1976) *Annu. Rev. Biochem. 45*, 11−37.
40. Streisinger, and Owen. (1985) *Genetics 109*, 633−659.
41. Kunkel, T. A. (1990) *Biochemistry 29*, 8003−8011.
42. Kunkel, T. A. (1992) *J. Biol. Chem. 267*, 18251−18254.
43. Schaaper, R. M., Koffel-Schwartz, N., and Fuchs, R. P. P. (1990) *Carcinogenesis 11*, 1087−1095.
44. Lambert, I. B., Napolitano, R. L., and Fuchs, R. P. P. (1992) *Proc. Natl. Acad. Sci. U.S.A. 89*, 1310−1314.
45. Garcia, A., Lambert, I. B., and Fuchs, R. P. (1993) *Proc. Natl. Acad. Sci. U.S.A. 90*, 5989−5993.
46. Shibutani, S., and Grollman, A. P. (1993) *J. Biol. Chem. 268*, 11703−11710.
47. Napolitano, R. K., Lambert, I. B., and Fuchs, R. P. P. (1994) *Biochemistry 33*, 1311−1315.
48. Grunberger, D., Nelson, J. H., Cantor, C. R., and Weinstein, I. B. (1970) *Proc. Natl. Acad. Sci. U.S.A. 66*, 488−494.
49. Fuchs, R. P. P., and Daune, M. (1971) *FEBS. Lett. 34*, 295−298.
50. O'Handley, S. F., Sanford, D. G., Xu, R., Lester, C. C., Hingerty, B. E., Broyde, S., and Krugh, T. R. (1993) *Biochemistry 32*, 2481−2497.
51. Heflich, R. H., and Neft, R. E. (1994) *Mutat. Res. 318*, 73−174.
52. Kraulis, P. J. (1991) *J. Appl. Crystallogr. 24*, 946−950.

BI9912138